Geodesy and Geodynamics xxx (xxxx) xxx

Contents lists available at ScienceDirect

Geodesy and Geodynamics

journal homepage: http://www.keaipublishing.com/geog

An enhanced spectral diversity coregistration method for dual-polarimetric Sentinel-1A/B TOPS data

Nan Fang [a], Xingjun Luo [a,*], Peng Shen [a], Lei Xie [a], Guoming Liu [b], Feixiang Wei [c], Kun Jiang [a], Wenbin Xu [a,**]

[a] Lab of Volcano and Earthquake Research, School of Geosciences and Info-Physics, Central South University, Changsha 410083, China
[b] Jilin Changbaishan Volcano National Observation and Research Station, Institute of Geology, China Earthquake Administration, Beijing 100029, China
[c] Institute of Geology, China Earthquake Administration, Beijing 100029, China

ARTICLE INFO

Article history:
Received 29 September 2022
Accepted 24 February 2023
Available online xxx

Keywords:
Coregistration
Terrain observation by progressive scans (TOPS)
Enhanced spectral diversity
Dual-polarization

ABSTRACT

Sentinel-1A/B data are crucial for retrieving numerical information about surface phenomena and processes. Coregistration of terrain observation by progressive scans (TOPS) data is a critical step in its application. TOPS data must be fundamentally co-registered with an accuracy of 0.001 pixels. However, various decorrelation factors due to natural vegetation and seasonal effects affect the coregistration accuracy of TOPS data. This paper proposed an enhanced spectral diversity coregistration method for dual-polarimetric (PolESD) Sentinel-1A/B TOPS data. The PolESD method suppresses speckle noise based on a unified non-local framework in dual-pol Synthetic Aperture Radar (SAR), and extracts the phase of the optimal polarization channel from the denoised polarimetric interferometric coherency matrix. Compared with the traditional ESD method developed for single-polarization data, the PolESD method can obtain more accurate coherence and phase and get more pixels for azimuth-offset estimation. In bare areas covered with low vegetation, the number of pixels selected by PolESD is more than the Boxcar method. It can also correct misregistration more effectively and eliminate phase jumps in the burst edge. Therefore, PolESD will help improve the application of TOPS data in low-coherence scenarios.

1. Introduction

Over the past two decades, Interferometric Synthetic Aperture Radar (InSAR) technology has gradually developed into an effective tool for monitoring surface changes. The increasing abundance of SAR satellite data strongly bolsters the development of InSAR technology. For instance, the Sentinel-1A/B data are released with free access and are widely utilized by researchers and engineers to study surface deformation efficiently [1]. Terrain observation by progressive scans (TOPS) observation mode was first applied to TerraSAR-X and now represents the standard observation mode for Sentinel-1A/B [2]. Notably, TOPS can achieve an observation width of 250km × 250km, thereby alleviating the problems of sector and azimuth variation in the conventional ScanSAR mode by controlling the antenna movement along the track direction [2].

Similar to the ScanSAR mode, the difficulties emerge from the large Dopplers that produce a significant coupling between the range and azimuth signals. The non-orthogonal acquisition geometry causes a phase ramp (including range and azimuth) in the impulse response functions for a squint angle. Thus, accurate coregistration of images acquired at different times is a key step in advancing the application of InSAR technology [3]. The premise for extracting interferometric signals in SAR images is coherence, which increases with coregistration accuracy. The phase ramp in azimuth introduces a phase bias if an azimuth is misregistered (i.e., so-called coregistration error). The phase bias can be expressed by:

$$\Delta\varphi = 2\pi f_{dc}\Delta t \tag{1}$$

where f_{dc} is the Doppler centroid, which is the average Doppler frequency, and Δt is the slow displacement [4].

* Corresponding author.
** Corresponding author.
E-mail addresses: luoxingjun@csu.edu.cn (X. Luo), wenbin.xu@csu.edu.cn (W. Xu).

Peer review under responsibility of Institute of Seismology, China Earthquake Administration.

Production and Hosting by Elsevier on behalf of KeAi

https://doi.org/10.1016/j.geog.2023.02.003

The azimuth shift limits the application of Sentinel-1A/B data in large-scale deformation monitoring. A coregistration accuracy of about 0.001 pixels is required to limit the azimuth shift to a few degrees. Prats-Iraola et al. [4] have proposed applying spectral diversity for the overlap region among bursts to address the azimuth shift problem driven by misregistration. This method has been called the enhanced spectral diversity (ESD). The general process of TOPS data coregistration includes two steps: (1) the initial coregistration based on geometry and (2) the coregistration by ESD [4].

The accuracy of the ESD mainly depends on the signal-to-noise ratio of the interference phase of the overlap region between sequential bursts [3]. In general, there are two ways to improve the accuracy of ESD. First, one can construct more robust coregistration networks for time-series SAR images to estimate the ESD phase using methods such as weighted least squares. The coregistration network includes Network-based ESD (NESD) based on temporal coherence and an improved network based on estimated coherence and graph theory [5–9]. Alternatively, one can improve the coherence of the overlap region in the following way. Sakar et al. [10] proposed an improved ESD method based on an estimator that utilizes all burst-wise and beam-wise overlap regions to refine a single common azimuth shift. Ma et al. [9] assumed the absence of decorrelation difference during the imaging time interval for the overlap region. In this way, the bias and variance can be reduced by combining two consecutive burst SLC samples. The same estimator has been successfully applied to the coregistration method based on the Dijkstra and all-pairs shortest path (APSP) networks [7,9]. The above methods for improving phase quality are all based on single-polarization (single-pol) data. Such methods often fail in images with prominent decoherence, such as scenes affected by vegetation or seasonality. To date, some studies successfully demonstrated surface deformation monitoring using the multi-polarimetric image, indicating that polarimetric InSAR has excellent potential in deformation monitoring [11].

As the principles of both ESD and interferometry are based on the coherence of SAR images, the traditional single-pol ESD method was improved by increasing the dual-polarization (dual-pol) interference phase in this study. The main aim is to increase the samples, and enhance the coherence, thereby increasing the coregistration accuracy of ESD. The primary contributions of this research are summarized as follows.

a) We present an ESD method for dual-Polarimetric (PolESD) TOPS data. The PolESD method suppresses speckle noise based on a unified non-local framework in dual-pol SAR and improves the interference performance of SAR images. Note that the interferometric phase, corresponding to the optimal polarization channel, was obtained by the Best method [12].
b) Our method is applied to typical low coherence scenarios and compared with traditional single-pol coregistration methods. The results show that the PolESD method has better coregistration accuracy than the traditional method.

2. Traditional single-polarization ESD method

The ESD method for coregistration only requires overlap regions, which significantly improves the efficiency of accurate coregistration. However, the ESD method has high sensitivity. To avoid the ESD phase wrapped, we use the primary and secondary SLC orbits and terrain height to generate an initial lookup table and then calculate the multi-look intensity images offset to achieve an initial coregistration accuracy of about 0.01 pixels.

We can assume that: (a) P and S are two images after initial coregistration, (b) they have the same Doppler centroid frequency f_c, (c) they share a standard bandwidth B, and (d) there is only constant misregistration between the images [3,4]. The ESD phase can be calculated for each overlap region as follows:

$$\varphi_{\text{err}} = arg\left\{ \left(P_i \cdot S_i^*\right) \cdot \left(P_{i+1} \cdot S_{i+1}^*\right)^* \right\} \tag{2}$$

where P_i and S_i refer to the i th primary and secondary complex bursts, and P_{i+1}, S_{i+1} refer to the $(i+1)$ th primary and secondary bursts; * indicates the conjugate operator, and $arg\{\cdot\}$ gives the phase of a complex number. The azimuth shift $\widehat{\Delta t}$ can be calculated as follows:

$$\widehat{\Delta t} = \underset{\Delta t}{argmax}\left\{ \left| \left(\sum_p e^{j\left(\varphi_{\text{err},p} - 2\pi\Delta f_{\text{ovl}}\Delta t\right)} \right) \right| \right\} \tag{3}$$

where Δf_{ovl} is the Doppler centroid frequency difference in the overlap region, Δt is a constant azimuth misregistration time. $\varphi_{\text{err},p}$ is the ESD phase for the candidate pixel p of each overlap region [6]. Therefore, the azimuth misregistration Δx of the overlaps of i and $i+1$ burst can be expressed by:

$$\Delta x = \Delta t/\tau = \varphi_{\text{err}}/2\pi\Delta f_{\text{ovl}}\tau \tag{4}$$

where τ is the azimuth time interval. As the estimation accuracy of φ_{err} is only related to the standard deviation of the noise phase, increasing the number of samples and improving the coherence can yield more accurate misregistration.

3. Improved ESD method based on dual-polarimetric data (PolESD)

This study mainly improved the traditional ESD-based method by enhancing the dual-pol interference phase. On the one hand, the speckle in the image can be more robustly reduced using the polarization-based method. On the other hand, the polarimetric optimal can select a better channel in the polarimetric space for exploitation. The principles of this method are described below.

3.1. Construction of polarimetric interferometric coherency matrix in overlap regions

For the dual-polarization Sentinel-1A/B TOPS data, in the sequential bursts, two overlap regions can be extracted from the primary and secondary images, respectively. They can be reflected by the Sinclair backscattering matrices as $\boldsymbol{P}_i$, $\boldsymbol{P}_{i+1}$, $\boldsymbol{S}_i$ and $\boldsymbol{S}_{i+1}$. For $\boldsymbol{P}_i$ and $\boldsymbol{S}_i$:

$$\boldsymbol{P}_i = \left[P_{i,\text{VV}}\ P_{i,\text{VH}}\right], \boldsymbol{S}_i = \left[S_{i,\text{VV}}\ S_{i,\text{VH}}\right] \tag{5}$$

Then, the four-dimensional polarimetric interferometric scattering target vector $\boldsymbol{k}_i$ can be obtained [13]:

$$\boldsymbol{k}_i = \left[\ P_{i,\text{VV}}\quad P_{i,\text{VH}}\quad S_{i,\text{VV}}\quad S_{i,\text{VH}}\ \right]^{\text{T}} \tag{6}$$

Calculating the outer product of $\boldsymbol{k}_i$ and its conjugate transpose, 4×4 polarimetric interferometric coherency matrix $\boldsymbol{T}_{i,\text{PolIn}}$ can be expressed by:

$$\boldsymbol{T}_{i,\text{PolIn}} = \left\langle k_i \cdot k_i^H \right\rangle = \begin{bmatrix} T_{11} & \Omega_{12} \\ \Omega_{12}^H & T_{22} \end{bmatrix} \tag{7}$$

where $\langle\cdot\rangle$ represents the set average of spatial homogeneous data, ^{H} indicates the conjugate transpose operator. Likewise, the polarimetric interferometric coherency matrix of $\boldsymbol{P}_{i+1}$ and $\boldsymbol{S}_{i+1}$ can be represented as $\boldsymbol{T}_{i+1,\mathrm{PolIn}}$.

3.2. Non-local means (NLM) for reducing speckle noise

Fundamentally, speckle noise is an inherent problem in InSAR. It generates a strong intensity fluctuation, hindering the image analysis and plaguing the estimation of interferometric properties. Hence, speckle noise reduction is essential in polarization data analysis.

The speckle reduction technique consists of two steps: 1) to identify homogeneous pixels (HPs) in a predefined or adaptive search window, and 2) to use the weighted average of the selected HPs. In this study, the NL-SAR introduced by Deledalle is proposed to reduce the speckle noise effectively and to estimate complex coherence robustly, given the unsupervised selection of filtering parameters [14].

The NL-SAR filter needs to perform a scaling operation on the non-diagonal elements of the matrix $\boldsymbol{T}_{\mathrm{PolIn}}$ to make it full rank, and use a spatial average-based prefilter to enhance covariance estimation before HP selection. For pixel x, the likelihood ratio test (LRT)-based patch matching is performed over all surrounding pixels x' in a large search window, and the satisfied pixels are taken as the HPs under a certain threshold. After mapping the weight $w(x,x')$ from the patch-wise similarity (based on an exponential kernel), the NLM estimator performs weighted averaging from the selected sample covariance matrices to suppress the detail-blurring effect.

$$\widehat{\Sigma}^{\mathrm{NL}}(x) = \frac{\sum_{x'} w(x,x')\boldsymbol{T}_{\mathrm{PolIn}}(x')}{\sum_{x'} w(x,x')} \tag{8}$$

where the full-resolution covariance matrix $\boldsymbol{T}'_{\mathrm{PolIn}}$ is used instead of pre-estimated covariances to preserve the image resolution.

To further reduce the signal non-stationarity induced by averaging the different populations, a bias-reduction step is then added after the NLM estimation by weighting between the non-local estimate and the original covariance matrix:

$$\widehat{\Sigma}^{\mathrm{NLRB}}(x) = \widehat{\Sigma}^{\mathrm{NL}}(x) + \alpha\left[\boldsymbol{T}_{\mathrm{PolIn}}(x) - \widehat{\Sigma}^{\mathrm{NL}}(x)\right], \tag{9}$$

$$\alpha = \max_{p}\left[\max\left(0, \frac{Var^{\mathrm{NL}}[I_p](x) - \widehat{I}_p^{\mathrm{NL}}(x)\big/L}{Var^{\mathrm{NL}}[I_p](x)}\right)\right]$$

where $\widehat{\Sigma}^{\mathrm{NLRB}}(x)$ is referred to as the non-local reduced bias (NLRB) estimate; weight α is computed using the intensity statistics of multiple polarimetric channels, L is the equivalent number of looks. $\widehat{I}_p^{\mathrm{NL}}(x)$ and $Var^{\mathrm{NL}}[I_p](x)$ are the weighted mean and variance of the intensity I_p at pixel x for channel $p \in \{1,2\}$, respectively. Note that the non-local estimate is retained when α is close to 0, and the original (noisy) empirical covariances are applied to replace the non-local estimate when the value is close to 1.

3.3. Best method

A necessary way to improve interference performance using polarization data is to select the optimal polarization channel according to the criteria. The best method is choosing the polarimetric channel that provides the highest coherence for each pixel [12].

In $\boldsymbol{T}_{i,\mathrm{PolIn}}$, the polarimetric coherence coefficients for the VV and VH channels can be quantified using (10):

$$\gamma_{i,\mathrm{VV}} = \frac{\Omega_{12}\{1,1\}}{\sqrt{\boldsymbol{T}_{11}\{1,1\}\boldsymbol{T}_{22}\{1,1\}}}, \gamma_{i,\mathrm{VH}} = \frac{\Omega_{12}\{2,2\}}{\sqrt{\boldsymbol{T}_{11}\{2,3\}\boldsymbol{T}_{22}\{2,2\}}} \tag{10}$$

The absolute value of the polarimetric coherence coefficient is the coherence, and the amplitude angle is the phase. The best method selects the one with more excellent coherence of the two complex coherence coefficients [12], and the corresponding interference phase is $\varphi_{i,\mathrm{best}} = arg(\gamma_{i,\mathrm{best}})$.

Likewise, for $\boldsymbol{T}_{i+1,\mathrm{PolIn}}$, the optimal polarimetric coherence coefficient $\gamma_{i+1,\mathrm{best}}$ and the corresponding phase $\varphi_{i+1,\mathrm{best}} = arg(\gamma_{i+1,\mathrm{best}})$ can be obtained. At last, the optimal coherence γ_{best} and ESD phase φ_{err} (misregistration) of the overlap region can be obtained by (11) and (12):

$$\gamma_{\mathrm{best}} = \left(\left|\gamma_{i,\mathrm{best}}\right| + \left|\gamma_{i+1,\mathrm{best}}\right|\right)\Big/2 \tag{11}$$

$$\varphi_{\mathrm{err}} = arg\left(\gamma_{i,\mathrm{best}} \cdot \gamma^{*}_{i+1,\mathrm{best}}\right) \tag{12}$$

Compared with the exhaustive search polarimetric optimization (ESPO) method in all polarization spaces, the best method selects the optimal unit complex vector in the existing polarization space. This allows for avoiding the huge computational burden and the instability that ESPO may encounter in the dual-polarization data.

This paper proposes an enhanced spectral diversity coregistration method for the dual-pol TOPS data (PolESD). The PolESD method allows accurate coregistration in the low-coherence scene. The flowchart of the PolESD method is shown in Fig. 1.

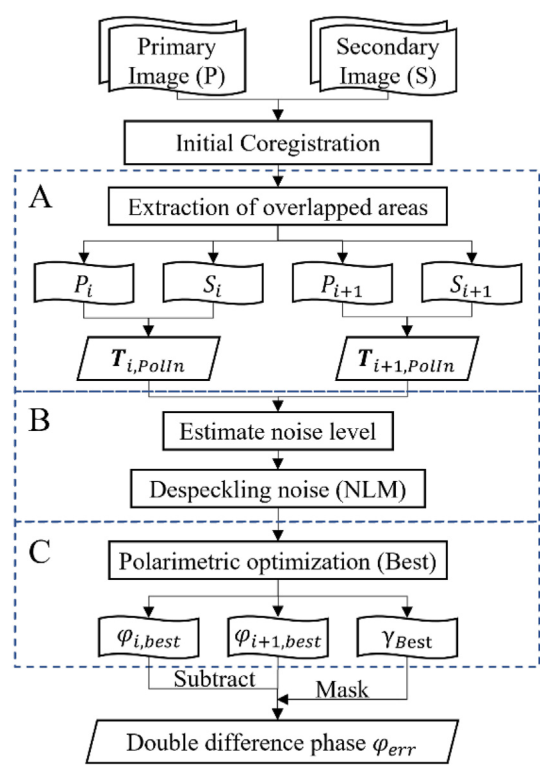

Fig. 1. Flow chart of the PolESD method based on polarized TOPS data.

First, the overlap region between the bursts was extracted from the primary and secondary images after initial coregistration. In Fig. 1, only two consecutive bursts are exemplified. The extracted overlap regions are $\boldsymbol{P}_i$, $\boldsymbol{P}_{i+1}$, $\boldsymbol{S}_i$ and $\boldsymbol{S}_{i+1}$. The matrix $\boldsymbol{T}_{i,\text{PolIn}}$ of the overlap region was constructed. A homogeneous region was extracted from the matrix to evaluate the noise, which was further used to reduce the speckle noise. The optimal polarization channel was extracted from the denoised matrix $\boldsymbol{T}_{i,\text{PolIn}}$ using the best method, alongside the corresponding coherence and phase. The ESD phase φ_{err} can be obtained by subtracting the masked phase, and the azimuth shift can be calculated by (4).

4. Data

Two dual-pol Sentinel-1A/B images (Descending, Path 134), covering the Tianchi Volcano (China/North Korea), were used to evaluate the effectiveness of the proposed method, and the coverage of the images is shown in Fig. 2. The perpendicular baselines of the image were 54 m, and the acquisition time was June 13, 2018, and June 25, 2018.

In the SAR images, the pixels that can be used for coregistration in the overlap regions are concentrated near the craters. These pixels represent areas covered by tundra or bare igneous rocks with an average elevation above 1700 m. Beyond this range, it is challenging to obtain a reliable phase due to the decoherence of volume scattering caused by vegetation coverage. Therefore, for TOPS data with vegetation cover, the coregistration accuracy depends on the phase estimation of small samples.

5. Experiment result and analysis

In this study, the polarimetric information was introduced for TOPS coregistration. The four experiments for comparison were established: (1) original (VV channel), (2) boxcar (VV channel), (3) NLSAR (dual-pol), (4) and PolESD. In the coregistration step, the overlap regions are usually multi-look for fast computation and to improve coherence. The multi-look operation tends to average the few pixels that have high consistency with surrounding pixels. Therefore, to avoid interference by multi-look, a full-resolution calculation is maintained in this study.

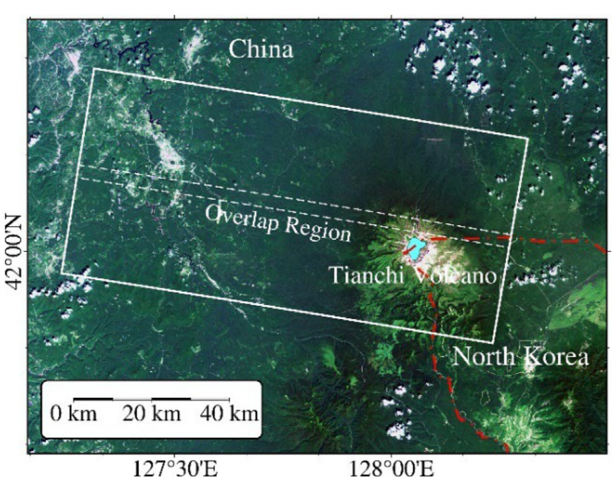

Fig. 2. The scope of the study area. The base map is an optical image acquired by the Sentinel-2 satellite in August (R: B4, G: B3, B: B2). The white dotted line indicates the overlap region shown in Figs. 3 and 4. The land cover in the overlap region is mainly vegetation, with only a few bare areas near the crater and a few buildings in the west of the overlap region.

The Boxcar method using a small window (few samples) would induce an overestimation of coherence in the low-coherence scene. When using coherence as the selection criterion, the Boxcar method results in a large number of noise pixels for analysis. Therefore, a Boxcar filter window size of 9 × 9 was selected in this study, which makes the coherence of the different methods comparable. Fig. 3 shows the coherence calculated by different methods. Without filtering, the coherence was equal to one (Fig. 3(a)). As seen from Fig. 3, the polarimetric-based method can more efficiently maintain the details in the image and improve the coherence.

Fig. 4 shows the phase after filtering by the four methods. As seen, all different methods significantly improved the phase quality. The phases in the red box show that clearer boundaries characterized the polarization-based approach. The coherence of the Boxcar method was slightly lower than the NLSAR or PolESD methods (Fig. 3), but the phase was smoother compared with the polarimetric-based methods.

In some scenarios, the effect of phase optimization is often reflected in the spatial continuity of the phase. However, it is challenging to evaluate whether the phase is accurate or not in detail by only using visual criteria, such as smoothness or roughness. This is especially true for the low-coherence area, where the spatial correlation of a few high-coherence pixels is unclear. Thus, for the TOPS coregistration, coherence and the ESD phase distribution can characterize the statistical quality of the phase.

From Fig. 5, the numbers of stable pixels selected in the building area by Boxcar, NLSAR and PolESD methods are 230, 355 and 370, respectively. The polarization-based method is better than the Boxcar method for selecting stable pixels, and NLSAR plays a

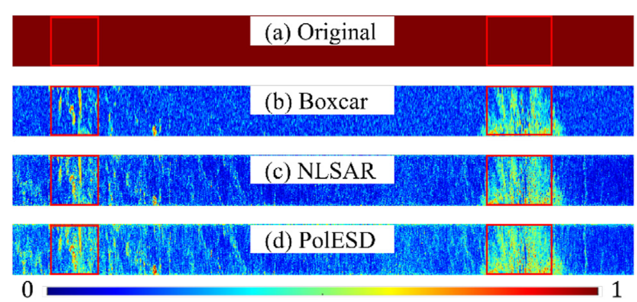

Fig. 3. Coherence estimated by different methods. The red box on the left contains a few building targets, and the red box on the right is the bare area of the crater.

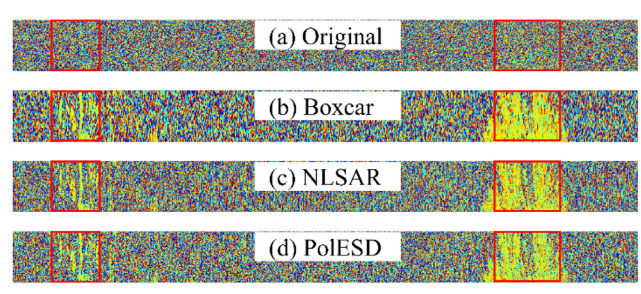

Fig. 4. The ESD phase estimated by different methods.

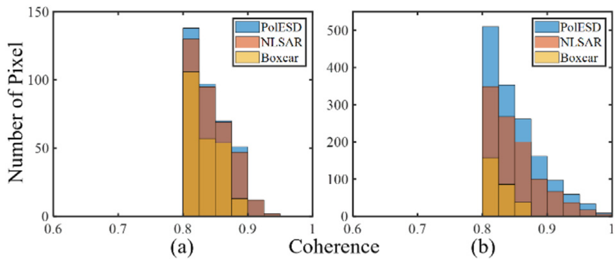

Fig. 5. Distribution of coherence, (a) and (b) correspond to the left and right red boxes in Figs. (3) and (4), which represent the low-density building area and the bare area, respectively.

significant role in improving the stable pixels. In bare areas covered with low vegetation, the number of pixels selected by the three methods is 281, 1054, and 1486. The number of pixels selected by PolESD is more than five times that of Boxcar. The number of high-coherence pixels indicates that the PolESD method can select far more pixels for estimating the ESD phase in natural scenes than the traditional method.

Fig. 6 shows the phase distribution in the red box in Figs. (3) and (4). From Fig. 6 (a), the phase distribution of the three methods is close, indicating that different methods have similar effects on selecting stable pixels. The phase distribution estimated by different methods is inconsistent in the bare area. The ESD phase estimated by the PolESD method in Fig. 6 (b) is 0.57, while the ESD phase estimated by Boxcar is 0.49. Taking the building area as a reference, the average ESD phase is 0.66. The phase difference estimated by PolESD in the bare area is only 0.09 rad, while the ESD phase estimated by the Boxcar method is 0.17 rad.

To further compare the correction performance of different methods, Fig. 7(a)-(e) show the original and the filtered uncorrected interferogram and the corrected interferogram by different methods.

From Fig. 7(b), the PolESD method accurately obtains the azimuth misregistration. It corrects the phase jump in the interferogram, while the Boxcar method has obvious phase jumps, indicating that it contains significant coregistration errors. From the section of burst edge (Fig. 8), the phase of this method is also smoother. Therefore, the PolESD method can effectively estimate misregistration.

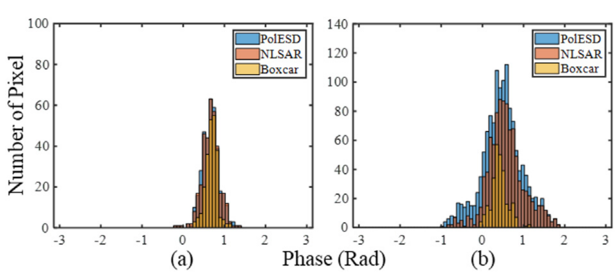

Fig. 6. Distribution of phase, (a) and (b) correspond to the left and right red boxes in Figs. (3) and (4), which represent the low-density building area and the vegetation or bare area, respectively.

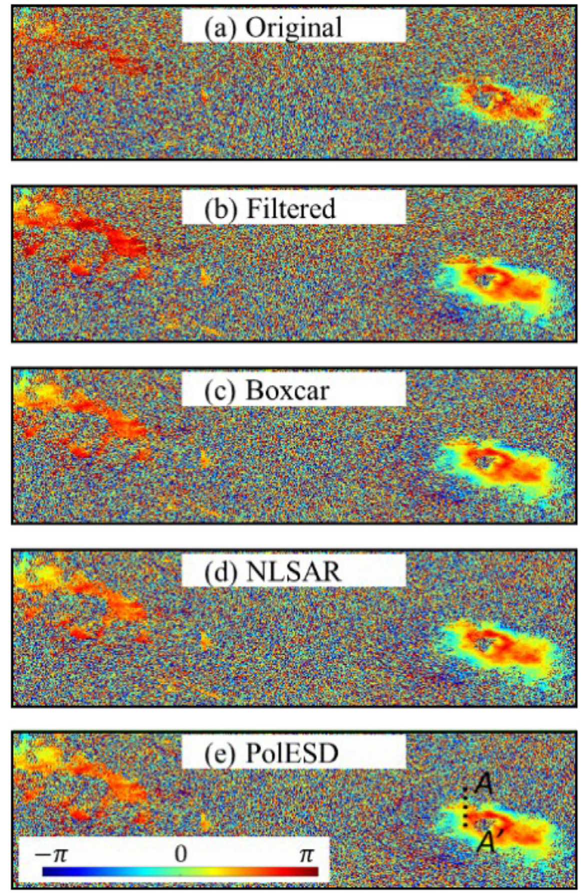

Fig. 7. (a) Uncorrected interferogram; (b) uncorrected interferogram after filtering; (c)–(e) are the interferograms corrected by different methods; $A-A$' is the section of Fig. 8.

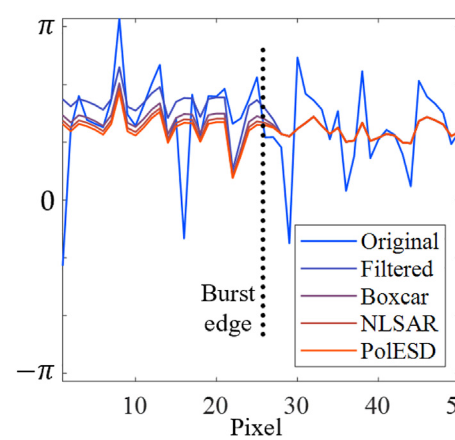

Fig. 8. The section of $A-A$' in Fig. 7, the black dashed line indicates the burst edge.

6. Conclusions

In this paper, we proposed the PolESD method to increase the coherence and phase quality in the overlap regions for dual-pol TOPS data. The PolESD method suppresses speckle noise based on a unified non-local framework. Then, the optimal polarization channel is extracted from the denoised polarimetric interferometric coherency matrix using the Best method. We demonstrate that the PolESD method can obtain more highly coherence pixels than the single-pol-based ESD method, and the PolESD method can obtain a more accurate ESD phase in the bare area.

Author statement

Nan Fang and Xingjun Luo designed the study, analyzed the results, and revised the manuscript; Nan Fang performed original draft and revised the manuscript; Lei Xie, Wenbin Xu, Peng Shen, Guoming Liu, and Feixiang Wei participated in analyzing the results and revising the manuscript. All authors have read and agreed to the published version of the manuscript.

Conflicts of interest

The authors declare that there is no conflicts of interest.

Acknowledgments

This work was supported by Jilin Changbaishan Volcano National Observation and Research Station (Project No. NORSCBS20-04), National Natural Science Foundation of China (42174023), and the Fundamental Research Fund for the Central Universities of Central South University (No. 506021722). The Sentinel-1 data were downloaded from the Alaska Satellite Facility (ASF) Distributed Active Archive Center (DAAC) website (https://vertex.daac.asf.alaska.edu/). Some of the figures were generated by Generic Mapping Tools (GMT 6.0.0) software (http://gmt.soest.hawaii.edu).

References

[1] P. Confuorto, et al., Sentinel-1-based monitoring services at regional scale in Italy: state of the art and main findings, Int J Appl Earth Obs Geoinf 102 (Oct. 2021), 102448, https://doi.org/10.1016/j.jag.2021.102448.

[2] F. De Zan, A.M. Guarnieri, TOPSAR: terrain observation by progressive scans, IEEE Trans Geosci Rem Sens 44 (9) (Sep. 2006) 2352–2360, https://doi.org/10.1109/TGRS.2006.873853.

[3] F. De Zan, P. Prats-Iraola, R. Scheiber, A. Rucci, Interferometry with TOPS: coregistration and azimuth shifts, Proc. Eur. Conf. Synth. Aperture Radar (2014) 949–952.

[4] P. Prats, L. Marotti, S. Wollstadt, R. Scheiber, TOPS interferometry with TerraSAR-X, Proc. Eur. Conf. Synth. Aperture Radar (2010) 44–47, https://doi.org/10.1109/TGRS.2011.2178247.

[5] H. Fattahi, P. Agram, M. Simons, A network-based enhanced spectral diversity approach for TOPS time-series analysis, IEEE Trans Geosci Rem Sens 55 (2) (Sep. 2016) 777–786, https://doi.org/10.1109/TGRS.2016.2614925.

[6] N. Yague-Martinez, F. De Zan, P. Prats-Iraola, Coregistration of interferometric stacks of sentinel-1 TOPS data, Geosci Rem Sens Lett IEEE 14 (7) (Jul. 2017) 1002–1006, https://doi.org/10.1109/LGRS.2017.2691398.

[7] M. Jiang, Sentinel-1 TOPS co-registration over low-coherence areas and its application to velocity estimation using the all pairs shortest path algorithm, J Geodes 94 (10) (Sep. 2020) 1–15, https://doi.org/10.1007/s00190-020-01432-1.

[8] X. Tian, Z.F. Ma, M. Jiang, A modification to time-series coregistration for sentinel-1 TOPS data, IEEE J Sel Top Appl Earth Obs Rem Sens 13 (May 2020) 1639–1648, https://doi.org/10.1109/JSTARS.2020.2985503.

[9] Z.F. Ma, M. Jiang, Y. Zhao, R. Malhotra, B. Yong, Minimum spanning tree Co-registration approach for time-series sentinel-1 TOPS data, IEEE J Sel Top Appl Earth Obs Rem Sens 12 (8) (Aug. 2019) 3004–3013, https://doi.org/10.1109/JSTARS.2019.2920717.

[10] N. Sakar, R. Brcic, F.R. Gonzalez, N. Yague-Martinez, An advanced co-registration method for TOPSAR interferometry, Proc. Int. Geosci. Remote Sens. Symp. (2015) 5240–5243, https://doi.org/10.1109/IGARSS.2015.7327016.

[11] S. Azadnejad, Y. Maghsoudi, D. Perissin, Evaluation of polarimetric capabilities of dual polarized Sentinel-1 and TerraSAR-X data to improve the PSInSAR algorithm using amplitude dispersion index optimization, Int J Appl Earth Obs Geoinf 84 (Feb. 2020), 101950, https://doi.org/10.1016/j.jag.2019.101950.

[12] R. Iglesias, D. Monells, X. Fabregas, J.J. Mallorqui, A. Aguasca, C. Lopez-Martinez, Phase quality optimization in Polarimetric differential SAR Interferometry, IEEE Trans Geosci Rem Sens 52 (5) (May 2014) 2875–2888, https://doi.org/10.1109/TGRS.2013.2267095.

[13] S.R. Cloude, Polarisation: applications in remote sensing, U.K., Oxford Univ. Press, Oxford, 2009 https://doi.org/10.1063/1.3502550.

[14] C.A. Deledalle, et al., NL-SAR: A unified non-local framework for resolution-preserving (Pol)(In)SAR denoising, IEEE Trans Geosci Rem Sens 53 (4) (Apr. 2015) 2021–2038, https://doi.org/10.1109/TGRS.2014.2352555.

Nan Fang received the B.S. degree from Wuhan University, Wuhan, China, in 2013, the M.Sc degree from the Hong Kong Polytechnic University, Hong Kong, China, in 2018. He is currently working toward the Ph.D. in geodesy from Central South University. His interests include SAR image processing and the joint inversion of earthquake source parameterss.

Xingjun Luo received the bachelor's degree from North China University of Science and Technology, Tangshan, China, in 2017, and the master's degree from Central South University, Changsha, China, in 2020. He is currently working toward the Ph.D. degree in geodesy and surveying engineering from Central South University, Changsha, China. His research interests include multi-temporal InSAR image processing and its applications on geophysical parameters inversion and motion mechanism interpretation.

Peng Shen received the bachelor's degree and the master's degree from the School of Geosciences and Info-Physics, Central South University, Changsha, China, in 2016 and 2019, where he is currently pursuing the Ph.D. degree in geodesy and surveying engineering. His research interests include Time-Series PolInSAR data processing and its applications on geosciences, including the statistical scattering signal modeling, homogeneous pixels selection-based spatial filtering, interferometric phase polarimetric optimization, phase linking theory, TSInSAR surface deformation monitoring, and PolInSAR forest parameter inversion technique.

Lei Xie received the bachelor's degree from China University of Geosciences, Wuhan, China, in 2014, the master's degree from the University of Calgary, Calgary, Canada, in 2018, and the Ph.D. degree in geodesy from the Hong Kong Polytechnic University, Hong Kong, China, in 2022. He is a lecturer at the School of Geosciences and Info-Physics, Central South University, Changsha, China. His research interests include InSAR, geodynamics, and applications in reservoir and dam systems.

Guoming Liu is a professor in Changbaishan Volcano Observatory, China. He is a seismologist who specializes in volcano seismology and geochemistry. His research interests are interaction between volcanoes and earthquakes, seismic velocity variation retrieved by ambient seismic noise, micro-earthquake detection and location.

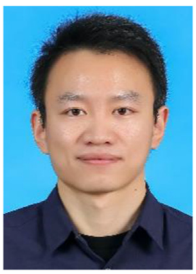

Feixiang Wei is an associate professor in the Institute of Geology, China Earthquake Administration. He is mainly engaged in volcano monitoring, volcanic gas and rock geochemistry.

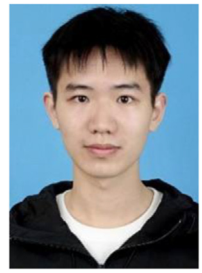

Kun Jiang received the bachelor's degree from the School of Geosciences and Info-Physics, Central South University, Changsha, China, in 2021, where he is pursuing the Ph.D. degree in geodesy and surveying engineering. His research interests include interferometric synthetic aperture radar and its applications on crustal deformation monitoring.

Wenbin Xu received the Ph.D. degree in Geophysics from King Abdullah University of Science and Technology, Saudi Arabia in 2015. He was a postdoc researcher with the Berkeley Earthquake Laboratory, University of California, Berkeley and an assistant professor with the Department of Land Surveying and Geo-Informatics, the Hong Kong Polytechnic University, Kowloon, Hong Kong. He is a professor and leads the Lab of Volcano and Earthquake Research in the School of Geoscience and Info-Physics, Central South University, Changsha, China. His research primarily focuses on the use of space geodesy to study ground deformation associated with a variety of geophysical and anthropogenic processes.